Int. J. Electrochem. Sci., 6 **(2011)** 4454 - 4469

International Journal of
ELECTROCHEMICAL
SCIENCE
www.electrochemsci.org

Carbon-Supported Platinum Molybdenum Electro-Catalysts and Their Electro-Activity Toward Ethanol Oxidation

H.D. Herrera-Méndez[1], *P. Roquero*[2], *M. A. Smit*[1], *L. C. Ordóñez*[1,*]

[1] Unidad de Energía Renovable, Centro de Investigación Científica de Yucatán, C. 43 No. 130 Col. Chuburná de Hidalgo, Mérida, Yucatán, CP 97200.
[2] Facultad de Química, Universidad Nacional Autónoma de México. Av. Universidad 3000 México D.F. CP 04510
[*]E-mail: lcol@cicy.mx

Received: 2 August 2011 / *Accepted:* 3 September 2011 / *Published:* 1 October 2011

We synthesized and studied a series of carbon-supported PtMo catalysts with a 20% metal loading as active phase. The analysis was made with three atomic ratios in the active phase, Pt-Mo: 1-1, 7-3 and 3-1. Samples were prepared by reducing metal precursor salts with formic acid. The materials were electrochemically characterized by cyclic voltammetry, current–sampled voltammetry, CO stripping voltammetry and electrochemical impedance spectroscopy. Physical characterizations were carried out by means of SEM-EDX and DRX. EDX analysis show that the atomic proportion between Pt and Mo is similar to the nominally proposed. DRX analysis allowed the identification of metallic Pt and different Mo oxides. The calculated average crystallite size was 4.7 nm. Electrochemical analysis revealed that the sample Pt-Mo 7:3 improves the catalytic activity of the anodic ethanol oxidation reaction, increasing the current density with low Pt loading and reducing the exchange charge resistance.

Keywords: PtMo/C, ethanol electro-oxidation, direct alcohol fuel cells

1. INTRODUCTION

Direct alcohol fuel cells (DAFC) are promising energy conversion devices that directly transform the chemical energy of a low molecular weight alcohol into electricity, through electro-catalytic reactions with higher efficiency than internal combustion systems. Ethanol is easily produced by different methods, among which fermentation and distillation of sugar rich organic materials is used worldwide. Ethanol possesses an energy density similar to that of gasoline (8 KWh/kg) [1] and its distribution, handling and storage could be made using the actual infrastructure with few modifications. For this reason it has been considered as a viable fuel to be used in fuel cells for

different portable power units. Systems operated with ethanol are named direct ethanol fuel cells (DEFC), since this compound is fed directly to the electrochemical system in liquid or gas form. The DEFC consist of an anode where ethanol is electro-oxidized to CO_2 and a cathode at which oxygen, generally from air, is reduced to form water. Both electrodes, usually based on platinum, are separated by a proton – conducting electrolyte. Nevertheless, as a consequence of the membrane acidity and the low operation temperatures (25 – 100 °C), rather poor kinetics of the ethanol oxidation reaction (EOR) are observed with platinum electrodes. The complete EOR occurring at the anode should yield 12 electrons mol^{-1}, according to:

$$C_2H_5OH + 3\ H_2O \rightarrow 2\ CO_2 + 12\ H^+ + 12\ e^- \qquad E^0_{anode} = 0.085\ V\ vs\ RHE\ [2]$$

However, this electrochemical reaction displays a complex mechanism with parallel and successive steps, with the formation of several intermediates such as CO, C1 and C2 species which adsorb strongly on the Pt surface, poisoning it in a wide range of electrode potentials. The main C2 species present are acetaldehyde at potentials below 0.6 V vs RHE and acetic acid at potentials higher than 0.8 V vs RHE, where the water molecule is activated to form oxygen – containing species at the platinum surface [2-6]. Therefore, in order to improve the efficiency of the DEFC, new anode catalysts are required to combine a high activity for ethanol oxidation and an improved tolerance towards intermediate species. Efforts to improve the activity and selectivity towards CO_2 have been focused in the incorporation of oxophilic metals such as Sn and Ru, and Mo [7, 8] that promote the activity of the catalyst in two ways: by activating water at low potentials or by modifying the electronic structure of the active phase [9]. Molybdenum trioxide is widely used as catalyst due to its structure that presents stacked layers of orthorhombic arrangements with each layer separated by Van Der Waals gaps [10]. The intercalation of hydrogen into the layered structure at the oxygen terminal sites produces five hydrogen molybdenum bronze phases (HxMoO3, $0<x<2$). At the crystal borders, OH^-, H^+ or OH_2 species may adsorb and desorb [10], and are thought to improve the oxidation of adsorbed intermediates [7].

Different types of bimetallic Pt-Mo electrodes have been prepared by means of very different methods [11-14]. Using an arc-melting furnace Dos Anjos et al [11] prepared Pt-Mo catalysts with compositions corresponding to an alloy (Pt:Mo 50:50) and to a solid solution (Pt:Mo 80:20), and found an ethanol oxidation enhancement on Pt–Mo electrodes compared with Pt-alone. The catalyst composition Pt–Mo (80:20) exhibited the best long term performance at steady-state potential. Levedeva and Jensenn [12] prepared carbon–supported Pt-Mo catalysts with a 60:40 molar relation by reduction of precursor salts ($Pt(NO_3)_2$ and $MoCl_5$) with formic acid or formaldehyde as reducing reagents. They found that Mo dispersion depends of the synthesis method and registered a low stability of the catalysts after electrochemical tests. Ordóñez et al. [13, 14] synthesized PtMo/C by platinum and molybdenum carbonyls thermolysis and obtained particles with an average size between 2 and 3 nm. The atomic ratio with the best performance for methanol oxidation was PtMo 4:1.

Some authors [7] have explained the catalytic promoter behavior of Mo by the bifunctional effect. According to Watanabe [15], the electro-dissociation of water on oxophilic elements, forming OH^- surface groups, occurs at lower potentials than on Pt, this OH^- surface groups oxidize the different

intermediate species adsorbed on adjacent Pt sites to yield CO_2. Chen et al [16] used density functional theory to calculate the effect of surface point defects of MoO_3 on the adsorption of different species. This oxide has three different types of Mo-O bonds, each one with different bonding energy. On the surface of the exposed plane, each oxygen vacancy is selective to adsorb different species such as H^+, OH^- or OH_2.

Other authors point to the hydrogen spillover effect to explain the EOR enhancement. In this phenomenon, a proton H^+ migrates from its adsorption site on Pt to a MoO_3 site, forming a hydrogen bronze [17], leaving the Pt active site available for adsorption of an ethanol molecule.

In this work, PtMo/C with different Pt:Mo molar ratios were synthesized using formic acid solutions as reduction agent of metallic precursors. In order to determine the activity enhancement for the ethanol electro oxidation reaction, all synthesized materials were tested in a three electrode electrochemical cell. For assessing the catalytic activity of different high surface area catalysts, the measured currents were normalized by the electrochemically active surface area of the material, which was determined by two different methods: adsorption-oxidation of CO (CO-stripping) and by the limit capacitance determination by electrochemical impedance spectroscopy. Physical properties were evaluated using SEM- EDX and DRX. This information was used to link the catalysts structure and the electrochemical performance.

2 EXPERIMENTAL

2.1 Synthesis

Table 1. Prepared Materials.

Catalysts	Mo content in active phase		Weight (%)		
	Atomic ratio Pt:Mo	R = Mo/(Mo+Pt)	Pt	Mo	C
Pt/C	1:0	0.00	20.0	0.0	80
Pt1Mo1/C	1:1	0.50	13.4	6.6	80
Pt7Mo3/C	7:3	0.30	17.2	2.8	80
Pt3Mo1/C	3:1	0.25	16.5	3.5	80
Mo/C	0:1	1.00	0.0	20.0	80

In accordance with the methodology proposed by Santiago et al [7], the synthesis of PtMo/C electrocatalyts was carried out by the reduction with 0.1 M formic acid solutions of precursor salts, perchlorplatinic acid (H_2PtCl_6) and/or tetrahydrated ammonium heptamolibdate ($(NH_4)_6Mo_7O_{24}$ $4H_2O$). Water type I (18 MΩ/cm) was used as solvent. Materials were supported on Vulcan XC72R carbon. In order to obtain a good adsorption of formic acid in the support pores, 800 mg of vulcan carbon were dispersed with vigorous agitation in 100 mL of 0.1 M formic acid solution for 1 h at 80°C. After, the appropriate quantities of precursor salts diluted in 50 mL of water were added drop by drop,

with agitation during 2 h. the catalysts were then separated and washed to eliminate the remaining chloride and ammonium ions. Afterwards, the obtained materials were dried at 100 °C for 12 h. Table 1 shows the prepared electrocatalysts. All of them were formulated with 80 wt % carbon and 20 wt% active phase in which the composition varied according to the atomic ratio: R=Mo/(Mo+ Pt) = 0, 0.25, 0.30, 0.75 and 1.00.

2.2 X Ray diffraction

Diffractograms were obtained at room temperature using Cu kα of 0.15406 nm radiation on a Siemmens 5000 diffractometer with a speed of 0.4 ° min^{-1}. Lattice parameters and platinum crystallite size were calculated by Bragg and Debye-Scherrer equations.

2.3 Scanning Electronic Microscopy

A variable operating pressure JEOL JSM—6360 LV scanning electron microscope, operated at 20 keV, equipped with electron dispersive X-ray (EDX) device was used for SEM-EDX studies. The presence of Pt and Mo was determined by the corresponding X-ray Kα characteristic lines. In order to determine the metal ratios, powder samples were fixed in a carbon tape and EDX- analyses were recorded in at least 10 points.

2.4 Electrodes preparation

A catalyst ink was prepared by mixing 5 μL of 2-propanol and 5 μL of a 10% w/w Nafion® solution (Sigma Aldrich) per mg of catalyst. The mixture was homogenized for 20 min in an ultrasonic bath. 5 μL of this ink were deposited onto a 5 mm diameter glassy carbon electrode. The catalyst loading corresponds to 1.27 mg cm^{-2} referred to the geometric surface area of the disk.

2.5 Electrochemical measurements

The electrochemical experiments were carried out at ambient temperature using an Autolab-PGSTAT 302N potentiostat-galvanostat with a FRA module. A typical three-electrode cell was used with a saturated mercury/mercurous sulfate electrode ($Hg/Hg_2SO_4/K_2SO_4$ (sat'd)) as reference, a graphite bar as counter electrode and each synthetized material as working electrode. All electrode potentials throughout this paper are referred to the reversible hydrogen electrode (RHE) scale. The working solution consisted of 1.0 M ethanol and 0.5 M H_2SO_4 as supporting electrolyte. Previous to carrying out the electrochemical tests, the catalytic materials were activated in a nitrogen-outgassed 0.5 M H_2SO_4 electrolyte, by potential cycling from 0.1 to 1.0V vs. RHE at a scan rate of 100 mVs^{-1} until no changes in electrical current were registered. During cyclic voltammetry (CV) measurements, the system was kept without stirring. All the potential sweeps in CV were first carried out towards positive

potentials, and then reversed towards negative potentials at scan rate of 10 mV s^{-1}. An electrochemical window from 0 to 1.6 V was investigated.

For CO stripping voltammetry, CO was adsorbed on the working electrode surface by fixing the potential at 100 mV for 1 h using a CO saturated 0.5 M H_2SO_4 working solution. The electrolyte was then replaced by a CO free, nitrogen-outgassed 0.5 M H_2SO_4 solution and CV tests were carried out in a potential window from 0 to 1.5 V vs. RHE at a scan rate of 10 mVs−1. The catalytic active area was calculated from the electrical charge of the CO oxidation peak, assuming the oxidation of a monolayer of linearly adsorbed CO on Pt sites, which corresponds to a 0.420 mCcm^{-2} charge [18-21]. Additionally, the active catalytic area was calculated from the limit capacitance according to the methodology proposed by Easton et al [22], in which a capacitance of 0.196 mF corresponds to 1 cm^2 of Pt surface. In this case, the catalytic ink was prepared with a concentration of 0.02 mg of catalyst/μL and 5 μL of this ink was deposited onto a 0.07 cm^2 glassy carbon electrode. Capacitance was recorded at 0.3 V vs RHE in 0.5 M H_2SO_4 solution with a frequency scan from 10 KHz to 0.1 Hz with an AC amplitude of 5 mV.

Current sampled voltammetry was carried out in a potential range from 0.0 up to 1.4 V vs RHE. The potential was fixed each 10 mV and current was registered during 30 s. Each stable current value was taken to build the I vs E plots. A 1.0 M ethanol + 0.5 M H_2SO_4 solution was employed in these tests. With the same working medium, electrochemical impedance spectroscopy (EIS) tests were collected in a potential window from 0.4 to 1.4 V vs RHE spaced at 0.1 V intervals and allowing 30 s for equilibration in each potential. The effective amplitude (rms values) of the AC signal employed was 5 mV and 50 frequencies from 10 KHz to 0.1 Hz were recorded at logarithmic intervals. NOVA 1.4 software was employed for data analysis.

3 RESULTS AND DISCUSSION

3.1 Physical characterizations

EDX elementary analysis results, as well as the crystallite size and the lattice parameter measured from DRX are listed in table 2.

Table 2. Physical parameters of PtMo/C series

Prepared catalysts	R_{theo}	EDX molar ratio	R_{Exp}	Lattice parameter a (Å)	Crystallite size (nm)
Pt/C	0.00	0.9 : 0	0.00	3.928	3.4
Pt3Mo1/C	0.25	2.9 : 1.1	0.28	3.919	5.6
Pt7Mo3/C	0.30	6.5 : 3.5	0.35	3.919	5.1
Pt1Mo1/C	0.50	0.8 : 1.2	0.60	3.919	4.7
Mo/C	1.00	0:1	1.00	N.D.	N.D.

EDX results of the bimetallic catalysts were obtained by analyzing different points of the sample. Pt:Mo atomic ratios were similar to the expected. Pt1Mo1/C shows the highest deviation probably due to the intrinsic variations of the synthesis method. However, because of the penetration depth of EDX analysis, some differences between surface and bulk compositions can exist. The crystallite size calculated by Scherrer equation ranges from 5.6 to 4.7 nm for PtMo/C materials, whereas for Pt/C it was 3.4 nm. No important changes were detected in the lattice parameter with the molybdenum incorporation.

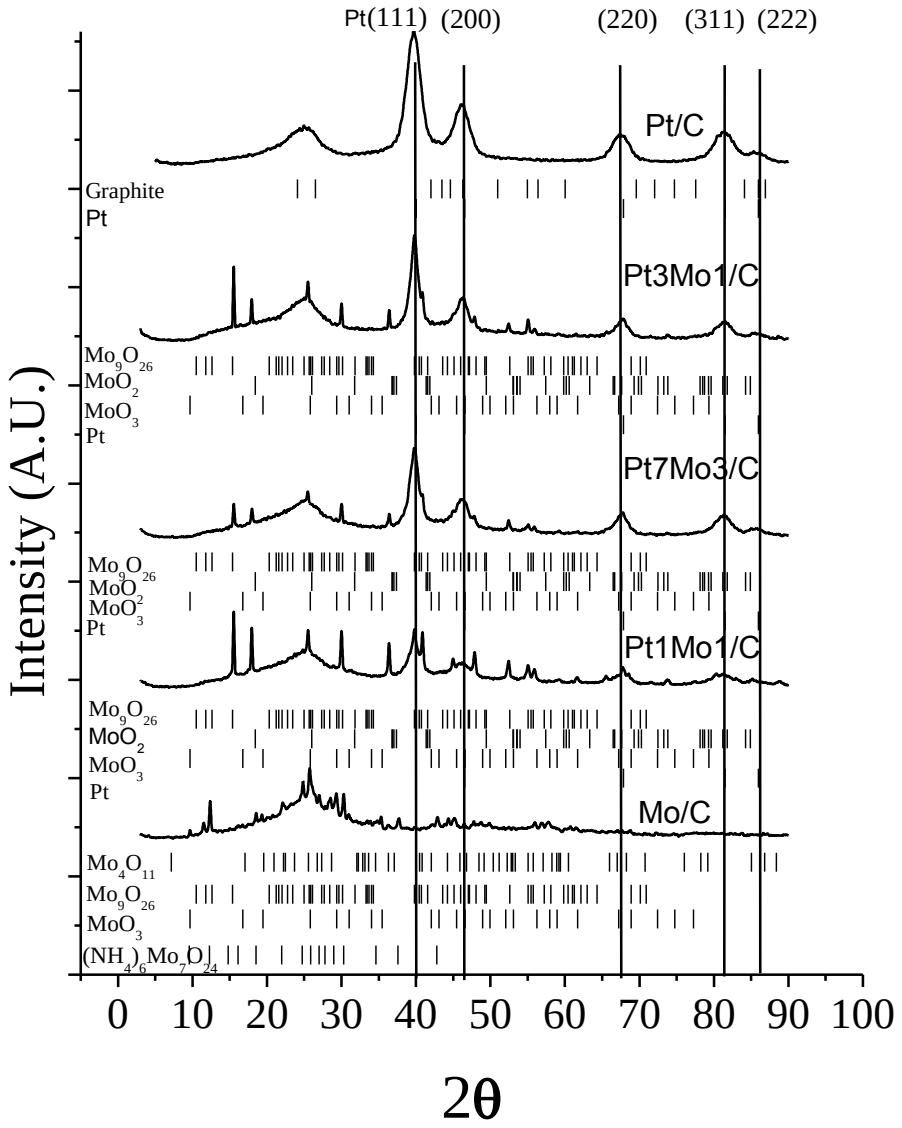

Figure 1. DRX analysis of PtMo/C series.

XRD patterns of PtMo/C materials are presented in figure 1. Pt/C exhibits sharp diffraction lines corresponding to the (111), (200), (220) and (222) planes of a fcc crystalline structure (card 04-0802). Additionally, it is possible to observe a small and broad diffraction peak at 25.9° attributed to the (002) plane of the hexagonal structure in the carbon support. On a fresh Mo/C sample, different

molybdenum compounds were identified, indicating an incomplete Mo oxidation: MoO_3 (card 21-0569), $Mo_9O_{26}On$ (card 05-0441), the Magneli phase Mo_4O_{11} (card 05-0337) and ammonium heptamolibdate (card 18-0117) remnants. In PtMo/C samples, the intensity of Pt lines increases with the Pt content, without any evident displacement related to the Mo content. Hence, it is not possible to conclude on the formation of a solid solution. The PtMo/C series presents peaks related to MoO_3, Mo_9O_{26} and MoO_2 (card 32-0671). Two significative lines corresponding to these oxides appear at 17.9 and 36.4° 2θ. The intensity of these signals is in the order Pt1Mo1/C > Pt3Mo1/C > Pt7Mo3/C. A lower intensity in this case could be related to a smaller particle size of Mo oxides.

3.2 Electrochemical measurements

3.2.1 Cyclic voltammetry

Voltammograms of Pt/C (figure 2) show the characteristic response of Pt in acid media.

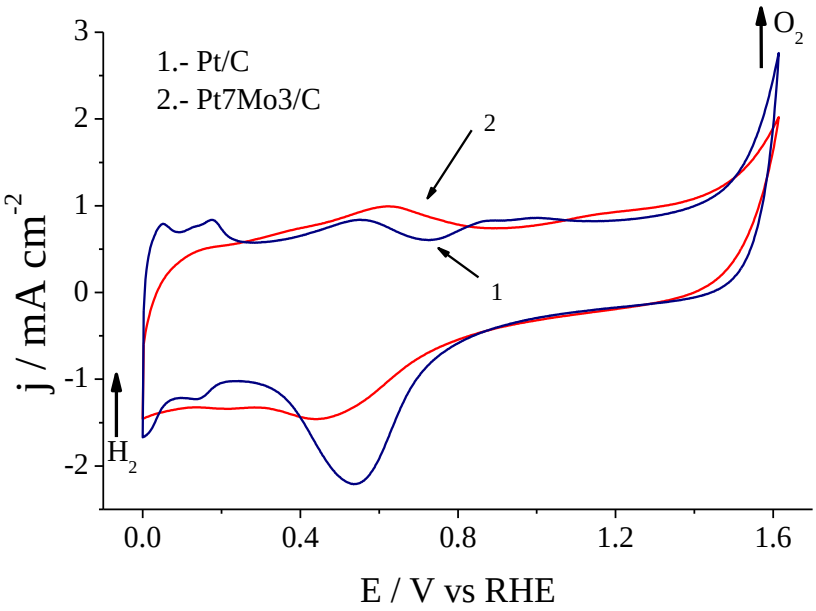

Figure 2. Cyclic voltammograms on [1] Pt/C and [2] Pt7Mo3/C in 0.5 M H_2SO_4 at a scan rate of 100 mVs^{-1}.

In the forward scan (towards positive potentials), between 0 V and 0.18 V are visible the anodic peaks corresponding to protons desorption from different planes of the platinum surface. At 0.55 V there is a peak associated to the oxidation of oxygen–containing groups of the carbon support [23]. At potentials higher than 0.7 V the formation of Pt hydroxides is observed, which are converted, at even higher potentials, into Pt(II) oxides. In the reverse sweep, Pt is reduced from Pt(II) to Pt^0, at potentials lower than 0.9 V with a maximum at 0.54 V. The proton adsorption on Pt surfaces can be observed at potentials smaller than 0.3 V, followed by the hydrogen evolution reaction. The Pt7Mo3/C sample does not present the proton desorption peaks because these are most probably incorporated into

the molybdenum trioxide structure forming molybdenum bronzes [24]. The Pt oxidation and reduction peaks presented lower currents due to the lower content of this metal in the formulation.

3.2.2 Electro-active area

In figure 3 are presented the first two cycles corresponding to the CO stripping test.

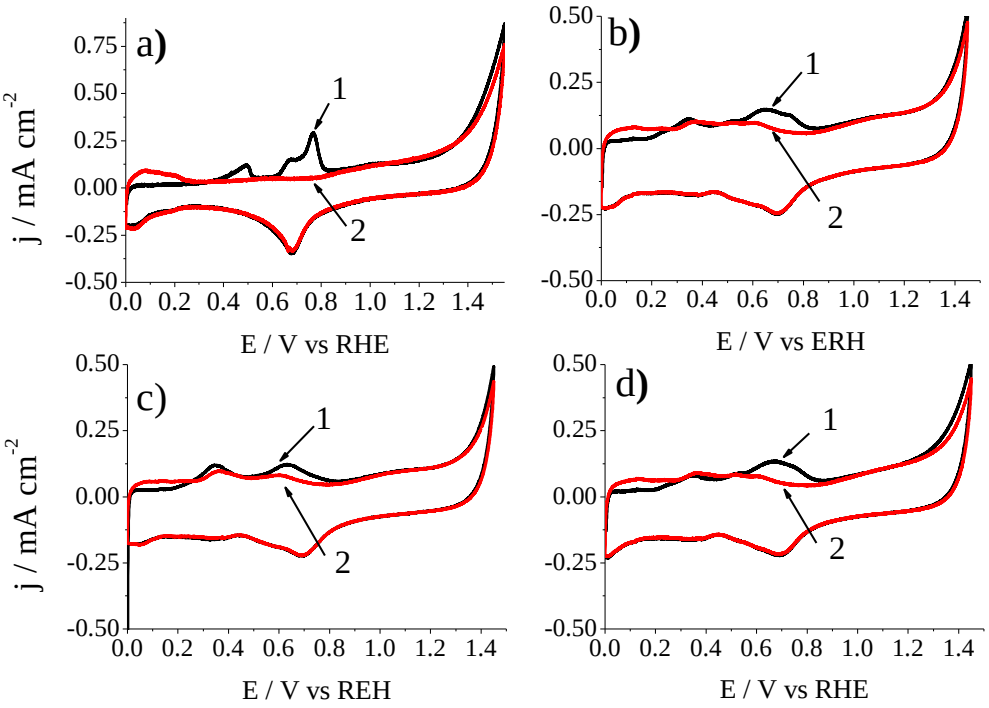

Figura 3. CO stripping on a) Pt/C, b) Pt3Mo1/C, c) Pt7Mo3/C, d) Pt1Mo1/C, at a scan rate of 10 mVs−1.

In the first cycle the proton desorption currents were lower than in second because the catalyst surface is covered with CO. Pt/C (figure 3-a) shows two CO stripping regions: the first one, corresponding to the oxidation of weakly adsorbed CO, starts at 0.32 V with peak potential at 0.49 V. The second region starts at 0.61 V and attains a shoulder at 0.67 V. These processes are due to oxidation of CO adsorbed with intermediate strength, possibly on (100) exposed Pt planes. Finally, at 0.76 V is observed the peak that corresponds to the oxidation of CO adsorbed with the highest strength [25]. In the return scan, Pt reduction, proton adsorption and hydrogen discharge are observed. The second cycle presents the typical behavior of Pt in the supporting electrolyte media. CO stripping on PtMo/C materials does not show the weak adsorption peak and the intensity and the transferred charge of the strongest adsorption is lower than on Pt alone. Pt3Mo1/C (figure 3-b) exhibits an onset potential for the CO oxidation peak at 0.61 V and a transferred charge of 29.72 μC. In Pt1Mo1/C electrocatalysts, the CO oxidation wave starts at 0.52 V with transferred charges of 14.7 μC. Pt7Mo3/C presented the lowest onset potential: 0.45 V with a charge of 9.15 μC, which could be

explained by the smaller crystallite size of oxidized Mo as it was observed by DRX. The Mo/C sample does not present the ability to adsorb or oxidize CO [13,21].

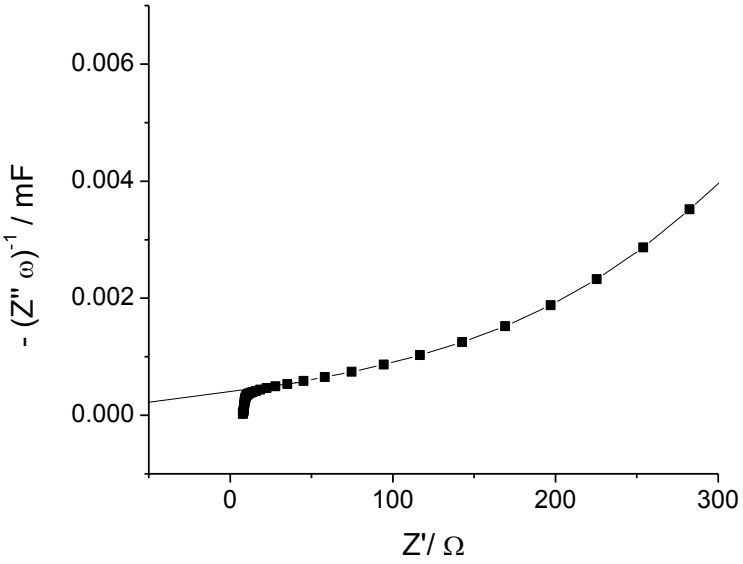

Figure 4. Capacitance plot of Pt3Mo1/C at dc bias of 0.3 V in 0.5 M H_2SO_4 solution.

Table 2. Estimated catalytic area by CO stripping and charge transfer resistances for ethanol oxidation by EIS.

Prepared catalysts	R	Active area m^2/g	Active area determined by EIS m^2/g	R_{ct} (Ω) At dc bias of 0.4 V	R_{ct} (Ω) At dc bias of 0.6 V
Pt/C	0.0	2.83	N.D.	706.1	792.7
Pt3Mo1/C	0.25	1.27	1.24	965.6	367.5
Pt7Mo3/C	0.30	0.87	0.84	689.2	378.8
Pt1Mo1/C	0.5	1.48	1.28	2484.1	2429.9
Mo/C	1.0	N.D.	N.D.	N.D.	N.D.

The catalytic active surface area (table 3) was calculated from the charge difference between the two cycles and assuming a 0.420 mC/cm^2 per monolayer of adsorbed CO [20]. There is not a straightforward relationship between active area and Mo content in the formulation. However, it might be related to the dispersion and crystallinity of the Mo oxides. MoO_3 core is completely saturated and is not available to adsorb CO and, apparently more dispersed Mo species could be blocking some Pt sites [26]. However, this proximity between Pt and MoO_3 results in an improved catalytic behavior, as revealed by the oxidation of adsorbed CO to CO_2 facilitated by the oxygen-containing species (-OH, OH_2) located at the borders of the octahedral molybdenum trioxide [10, 26]. Figure 4 presents the capacitance vs real impedance of Pt3Mo1/C catalysts at dc bias of 0.3 V in 0.5 M H_2SO_4 solution. The total capacitance includes both, double layer capacitance and faradic pseudo capacitance terms for

both, active phase and carbon support. According to Easton et al [22] the limiting capacitance correlates to the active area assuming that, at this potential, the capacitance of the double layer does not vary and that 0.196 mF corresponds to 1 cm^2 of 20% Pt on C. Following their methodology, the electro active area of the PtMo/C series was calculated (table 3) with good agreement to that calculated from CO stripping. The active area was used to normalize the signals of electro-oxidation studies.

3.2.3 Ethanol electro-oxidation studies

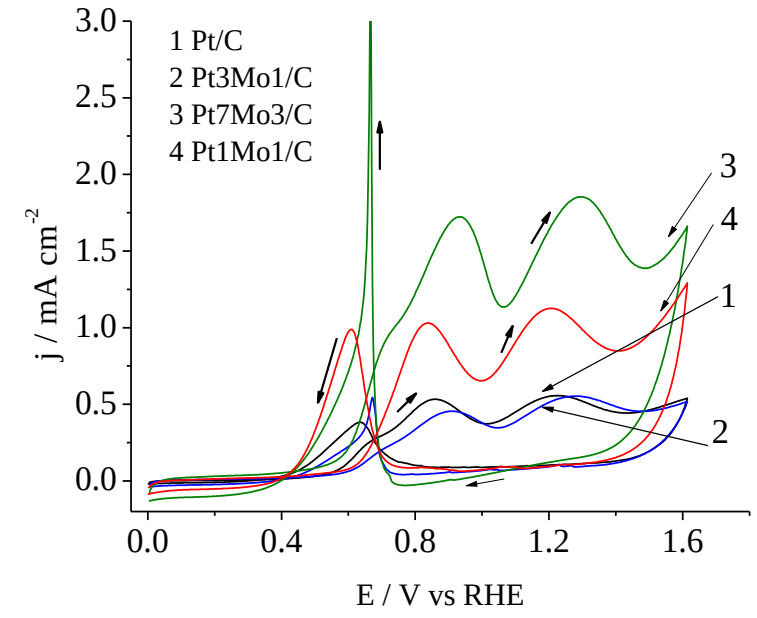

A

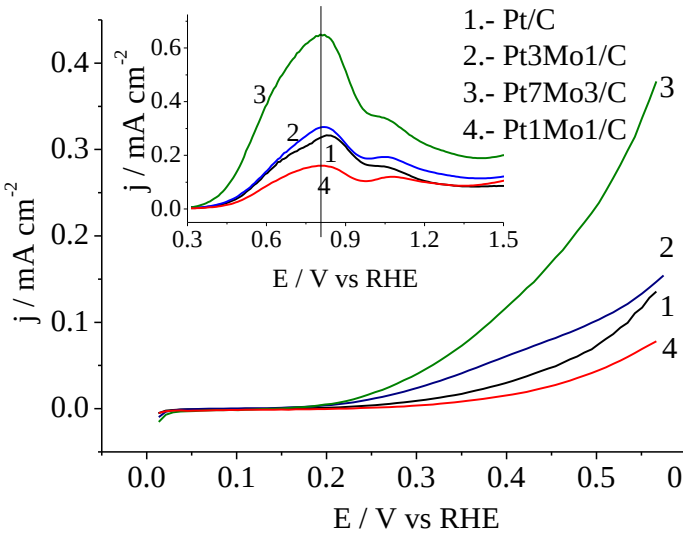

B

Figure 5. a) CV at 10 mV/s and b) Current sampled voltammetry of PtMo/C series in 1.0 M CH_3CH_2OH + 0.5 M H_2SO_4.

Figure 5a presents the voltammetric profiles from the PtMo/C series. These experiments were recorded with a 10 mV/s scan rate, in a 1.0 M ethanol + 0.5 M H_2SO_4 solution. In the scan towards positive potentials two oxidation processes are observed. The first one corresponds to acetaldehyde formation, beginning in 0.4 V, with a maximum for Pt/C in 0.9 V (peak A) [4],

$$CH_3 — CH_2OH + Pt \rightarrow Pt(CH_3\text{-}CH\text{-}OH)_{ads} + H^+ + e^-$$

$$Pt(CH_3\text{-}CH\text{-}OH)_{ads} + H_2O \rightarrow Pt + CH_3{-}CHO + H^+ + e^-$$

The second one (peak B, figure-5a) is associated to acetic acid formation and starts for Pt/C at 1 V with peak potential at 1.2 V. For this reaction, OH^- groups are necessary from the electrochemical water dissociation carried out at Pt sites, and therefore, it occurs at potentials higher than 0.8 V. [4]

$$(CH_3 — CHO)_{ads} + Pt\text{-}OH_{ads} \rightarrow Pt + CH_3 — COOH + H^+ + e^-$$

At about 0.7 V a shoulder corresponding to the water electrochemical activation is observed.

$$Pt + H_2O \rightarrow Pt\text{-}H_{ads} + Pt\text{-}OH_{ads}$$

Finally at 1.3 V the oxygen evolution is observed. In the reverse scan, anodic currents are observed between 0.8 and 0.5 V. The slope change for this process is to note and it is characteristic of the oxidation of adsorbed organic species. This anodic current starts at a potential very close to that of the oxidation state changes for Pt(II) to Pt^0, because of this, the desorbed oxygen participates in the oxidation of the intermediate organic species to CO_2.

From the results of the entire series, it is evident that Pt7Mo3/C presents the lowest onset potential (0.49 V against 0.55 V for Pt/C) and the highest current density for the ethanol oxidation reaction, 1.72 mA/cm^2 against 0.53 mA/cm^2 for Pt/C in peak A, and also for the other two peaks. A good electrocatalysts must fulfill at least two requirements: 1) high current density and 2) lower onset potential for the corresponding electrochemical process. According to this, Pt7Mo3/C presents the highest ethanol electro-oxidation activity.

With the aim of studying the EOR with a reduced participation of currents associated to capacitive process, the current - sampled voltammetry (figure 5b) was carried out under the conditions described above. It is possible to observe clearly that the acetaldehyde formation is favored at steady state conditions. There is a not significant difference in the onset potential for the entire PtMo/C series. However, at low potentials the slope of the I-E curve is in the order: Pt7Mo3/C > Pt3Mo1/C > Pt/C > Pt1Mo1/C. At about 0.7 V this tendency slows down for Pt/C and Mo1Pt1/C, because Pt/C has most of its active sites blocked with adsorbed intermediates, and the oxidation reaction cannot proceed until water is electro-dissociated at higher potentials. In the case of Pt1Mo1/C, the reaction rate slowdown is due to the low Pt content. For PtMo/C materials, the main peak appears at lower potentials than in the case of Pt/C. Low Mo contents in the formulation results in a better EOR performance because in these materials the water electro activations occurs at lower potentials than in Pt/C.

3.2.4 Electrochemical impedance spectroscopy

Figure 6a shows the complex plane plots of Pt/C obtained in a potential range from 0.4 to 1.4 V, using the supporting electrolyte solution, 0.5 M H_2SO_4.

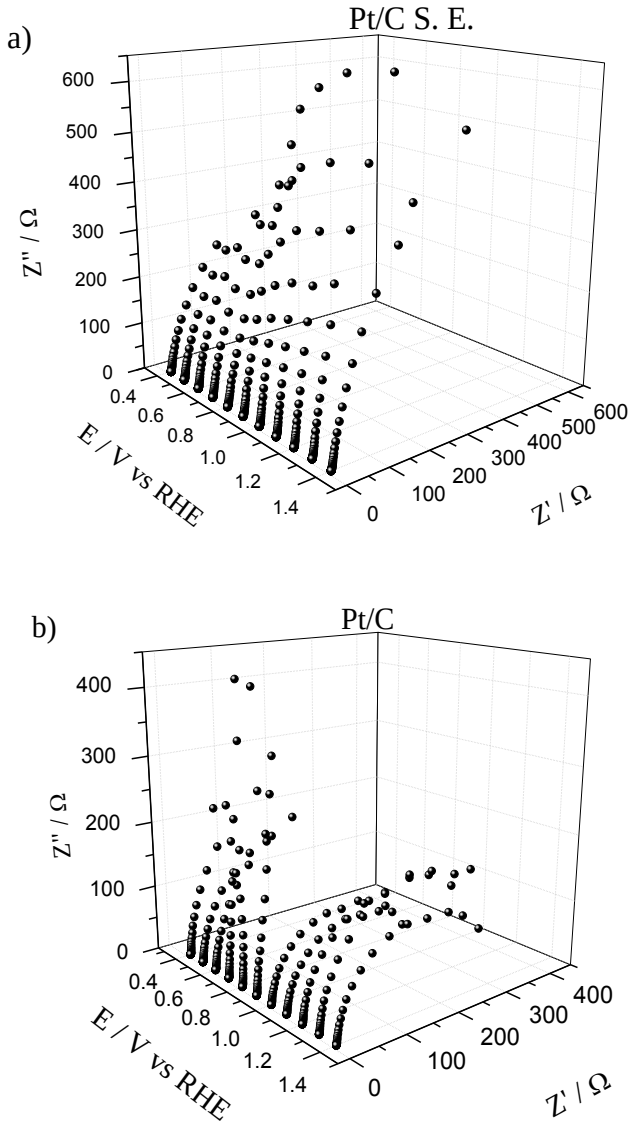

Figure 6. Complex plane impedance plot of Pt/C at various electrode potentials in: a) support electrolyte and b) 1.0 M CH_3CH_2OH + 0.5 M H_2SO_4.

At low potentials (0.4 V – 0.7 V) defined semicircles are observed, which at potentials superior to 0.8 V presented wider diameters, attributed to the oxidation changes from Pt^0 to Pt(II), and having as consequence, an increase of the capacitive charge of the electrode-electrolyte interface. Using the working solution, 1.0 M CH_3CH_2OH + 0.5 M H_2SO_4 (figure 6b) important variations are appreciated. At lower potentials, semicircles presents a high diameter and it increase due to the intermediate species formation through the different trajectories of the EOR mechanism. In the range of 0.6V – 0.8 V there

is a noticeable inductive behavior associated to the change of the electrode surface by the water electro-dissociation reaction and Pt oxidation. Afterwards, more defined cycles are observed related to an easier oxidation of species such as acetaldehyde or acetic acid.

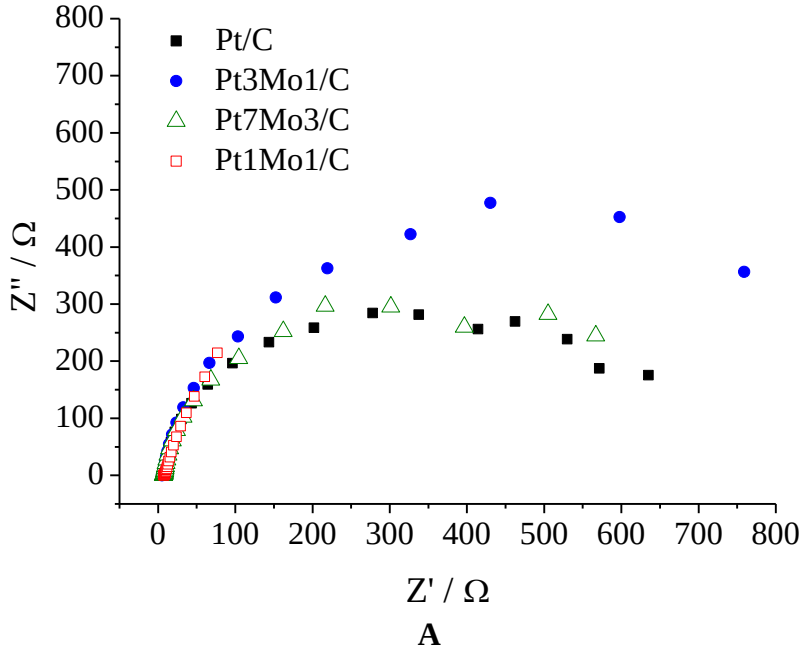

A

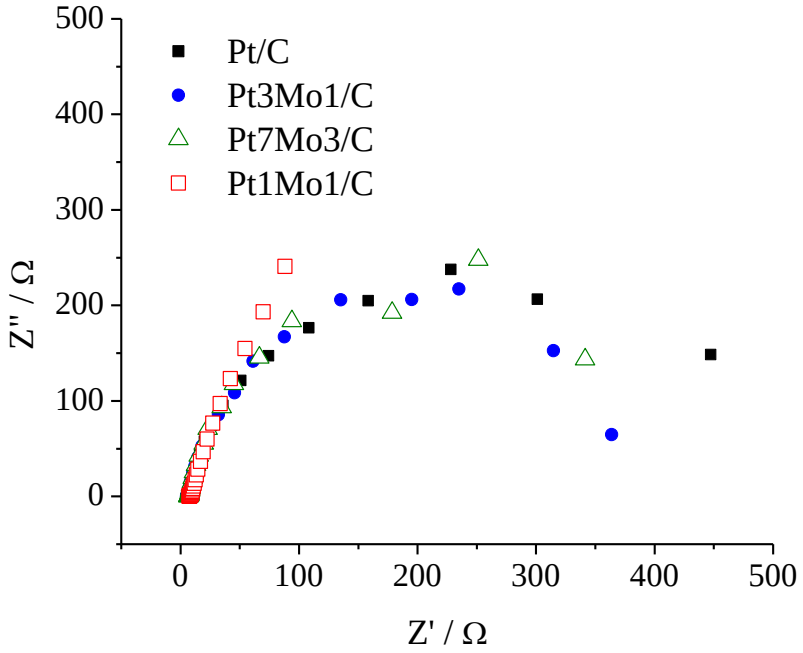

B

Figure 7. EIS measurements of PtMo/C series in1.0 M CH_3CH_2OH + 0.5M H_2SO_4 solution at dc bias of A) 0.4V and B) 0.6V.

To compare the electrochemical activity of the PtMo/C materials, the transfer charge (R_{CT}) was calculated from the diameter of semi-circles in the complex plane impedance plot (figure 7). Data was fitted to an equivalent circuit (figure 8). This circuit consists of a resistor that represents the solution and ohmic losses, R_S, in combination with a parallel arrangement of a constant phase element (CPE) and a resistor related to the charge transfer (R_{CT}) across the electrode-electrolyte interface [1].

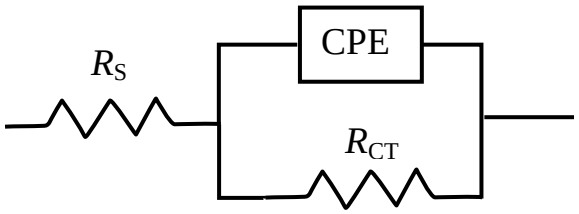

Figure 8. Equivalent circuit of the ethanol electro-oxidation at PtMo/C electrocatalysts.

The potentials for this study (0.4 and 0.6 V) were selected because they correspond to the onset of the EOR and thus the catalytic surface is expected to be covered with the formed intermediate species (figure 7). At 0.4 V the tendency of R_{CT} (table 3) was Pt7Mo3/C > Pt/C > Pt3Mo1/C >> Pt1Mo1/C. At 0.6 the tendency was Pt7Mo3/C ≈ Pt3Mo1/C > Pt/C > Pt1Mo1/C. This change in the tendency it may be due to the fact that, at 0.4 V intermediate species are still in formation and, as potential rises, intermediate species are completely formed and the promoter effect can be observed as a decrement in R_{CT}.

4. CONCLUSIONS

The synthesis method by reduction with formic acid allowed to obtain Pt particle with sizes between 3 and 6 nm and Pt:Mo proportions close to those proposed. Pt/C and PtMo/C materials do not present diffraction lines displacements of the Pt fcc crystalline structure, and no important changes were detected in the lattice parameter with the molybdenum incorporation, indicating that no alloy or solid solution were formed. Fresh PtMo/C samples presented different stoichiometric oxides (MoO_X, where $2<x<3$). In this way, the catalytic surface was composed of Pt particles separated from Mo species.

As indicated by the CO stripping test, no strong adsorption peaks were found with PtMo/C materials and the CO oxidation occurs at lower potentials than Pt/C. It represents a higher tolerance to the presence or formation of this intermediate species.

From current-sampled voltammetry results, it is evident that PtMo/C materials favor the acetaldehyde path of the EOR mechanism. It was also possible to observe higher current densities and a higher slope tendency with low Mo contents at the onset of the EOR. Lower current peak values from PtMo/C materials than Pt/C were also observed.

Electrochemical impedance spectroscopy reveled surface capacitance changes at different potentials related to changes in the Pt oxidation state. At the onset of the EOR, Pt7Mo3/C exhibits

higher activity than Pt/C. However, when potential rises and the electrochemically active surface is covered with intermediate species, the activity of the low Mo content materials is improved, as shown by the R_{CT} changes between 0.4 and 0.6 V. This is to be attributed to the Mo promoting effect, even though the catalytic area of Pt7Mo3/C is smaller than those of Pt/C and Pt3Mo1/C, as expected, its performance was close to that of the Pt/C material, with lower Pt content.

Differences in the Pt7Mo/C and Pt3Mo1/C activities at low potentials can be explained in terms of the Mo dispersion or of its oxidation degree, in accordance with the observed intensities of the diffraction lines.

ACKNOWLEDGEMENTS

The authors thank Tanit Toledano and Santiago Duarte for SEM-EDX, Daniel Aguilar for technical assistance in DRX analysis, Gustavo Martínez and Jorge Domínguez for technical support. The authors acknowledge the financial support for this work from CONACyT (projects 58332 and 116157). H.D. Herrera-Méndez thank CONACyT for grant No. 224224. Facultad de Química-UNAM is gratefully acknowledged for the investigations on CO tolerance on PtMo/C electrocatalysts.

References

1. S. Gupta, J. Datta, *J Chem Sci* 4 (2005) 337-344
2. F. Vigier, S. Rousseau, C. Countanceau, J.M. Leger, C. Lamy, *Top Catal* 40 (2006) 1-4
3. H. Hitmi, E.M Belgsir, J.M Leger, C. Lamy, R.O. Lezna, *Electrochim Acta* 39 (1994) 407-415
4. C. Lamy, E. M. Belgsir, J. M. Léger, *J Appl Electrochem* 31 (2001) 799-809
5. B. Hoyos, J. Gonzalez, C. Sanchez, *Dyna* 136 (2002) 31-40
6. G.A Camara, R.B.de Lima,T. Iwasita, *Electrochem Commun* 6 (2004) 812-815
7. E.I Santiago, G.A. Cámara, E.A Ticianelli, *Electrochim Acta* 48 (2003) 3527-3534
8. E. Antolini, *J Power Sources* 170 (2007) 1-12
9. W.J. Zhou, B. Zhou, W.Z. Li , Z.H. Zhou, S.Q. Song, G.Q. Sun, Q. Xin, S. Douvartzides, M. Goula , P. Tsiakaras, *J Power Sources* 126 (2004) 16-22
10. S. Adams, *J Solid State Chem* 149 (2000) 75-87
11. D.M. Dos Anjos, K.B. Kokoh, J.M. Léger, A.R. De Andrade, P. Olivi, *J Appl Electrochem* 36 (2006) 13491-1397
12. N.P Levedeva, G. J. M. Janssen, *Electrochim acta* 51 (2005) 29-40
13. L.C Ordóñez, P. Roquero, P.J. Sebastian, J. Ramírez, 2005, *Catal Today* 107-108 (2005) 46-52.
14. P. Roquero, L.C. Ordoñez, O. Herrera, O. Ugalde, J. Ramirez, *Int J Chem React Eng* 5 (2007) 1-9
15. M. Watanabe, S. Motoo. *J Electroanal Chem* 60 (1975) 267-273
16. M. Chen, C.M. Friend, E. Kaxiras, *J Am Chem Soc* 123 (2001) 2224-2230
17. J. G. Kim, J. Z. Shyu, J. R. Regalbuto, *J Catal* 139 (1993) 153-174
18. W. H. Lizcano-Valvuena, V.A. Paganin, C.A.P. Leite, F. Galembeck, E. R. Gonzalez, *Elecrochim Acta* 48 (2003) 3869
19. Y. Takasu, T. Kawaguchi, W. Sugimoto, Y. Murakami, *Electrochim Acta* 48 (2003) 3861
20. O.V. Cherstiouk, P.A. Simonov, V.I. Zaikovskii, E.R. Savinova, *J Electroanal Chem* 554-555 (2003) 241-215
21. L.C. Ordoñez, P. Roquero, P.J. Sebastian, J. Ramirez, *Int J Hydrogen Energ* 32 (2007) 3147 – 3153

22. E. B. Easton, P. G. Pickup, Electrochim Acta 50 (2005) 2469-2474
23. J.L. Figuereido, M.F. Pereira, M.M. Freitas, J.J. Orfao, *Carbon* 37 (1999) 1379-1389.
24. R. Smith, G. Rohrer, *J Catal*, 173 (1998) 219-228
25. G. Samjeske, H. Wang, T. Löffler, H. Baltruschat, *Electrochim Acta* 47 (2002) 3681-3692
26. Z. Jiang, W. Huang, H. Zhao, Z. Zhang, D. Tan, X. Bao, *J Mol Catal A-Chem* 268 (2007) 213–220
27. S. P. Mehandru, A. B. Anderson., *J Am Chem Soc* 110 (1988) 2061-2065.